JOURNAL OF MATERIALS SCIENCE **38** (2003) 2373–2391

Microstructural evolution of simulated heat-affected zone in modified 2.25Cr-1Mo steel during high temperature exposure

M. C. TSAI*, C. S. CHIOU†, J. R. YANG*
Institute of Material Science and Engineering, National Taiwan University, 1 Roosevelt Rd., Sec. 4, Taipei, Taiwan, ROC
E-mail: jryang@ccms.ntu.edu.tw

The effect of heat input with 20, 50 and 80 kJ/cm on the microstructural evolution of the simulated heat affected zone (HAZ) has been studied in a modified 2.25Cr-1Mo steel. The microstructures of simulated coarse-grained HAZ has been examined by optical metallography and transmission electron microscopy. It was found that large amounts of martensite with small quantities of bainite exist in the specimen with 20 kJ/cm. However, significant amount of bainite with a few amounts of allotriomorphic ferrite can be detected in the specimen with 50 kJ/cm heat input. In the case of heat input with 80 kJ/cm, the simulated HAZ microstructures were composed chiefly of bainite with a few amounts of martensite and allotriomorphic ferrite. In order to study the sequences of carbide transformation, the HAZ specimens were tempered at 700°C for different intervals (1, 2, 5, 10, 20, 50, 100, 200 and 500 h). The sequence of carbide transformation in the HAZ zone of this modified 2.25Cr-1Mo steel has been proposed.

1. Introduction

Modified 2.25Cr-1Mo steel has been developed from the 2.25Cr-1Mo steel for more than two decades [1]. This type steel has a negligible silicon concentration (0.05 wt%), a lower carbon concentration (0.1 wt%) and the additional solutes 0.25V-0.02Ti-0.002B (wt%). It has been found to exhibit an improved creep strength and impact toughness to achieve higher process efficiencies in coal conversion plants, chemical processing plants and petrochemical refining plants [2].

Mo and Cr are the main elements in Cr-Mo steels because they can form more stable carbides (such as M_7C_3, M_2C , $M_{23}C_6$, etc.) to support the creep resistance ability when used at elevated temperatures (400–700°C) for a long period. In addition, when phosphorous exists in matrix, Mo is to suppress embrittlement by scavenging of P, presumably by a Mo-P compound formation, thereby diminishing P segregation [3]. The microalloying Mo has the great effect on the elevated properties in modified 2.25Cr-1Mo steel. On the other hand, carbon content is restricted to 0.1 wt% so as to avoid possible welding problems. Silicon content is about 0.02 wt% which is less than that in typical 2.25Cr-1Mo steel (0.2–0.4 wt%). The reason for reduction of silicon is to increase resistance to the tempered embrittlement at elevated temperatures. The addition of vanadium can improve the elevated-temperature strength, since vanadium carbides are presumably more stable than the chromium and molybdenum carbides. Addition of boron with 0.002 wt% is credited with increasing the hardenability of the alloy, allowing for the formation of martensite or bainite or a mixture of the two at a lower cooling rate. The main function of titanium is to tie up nitrogen, so that boron is not removed from solution as

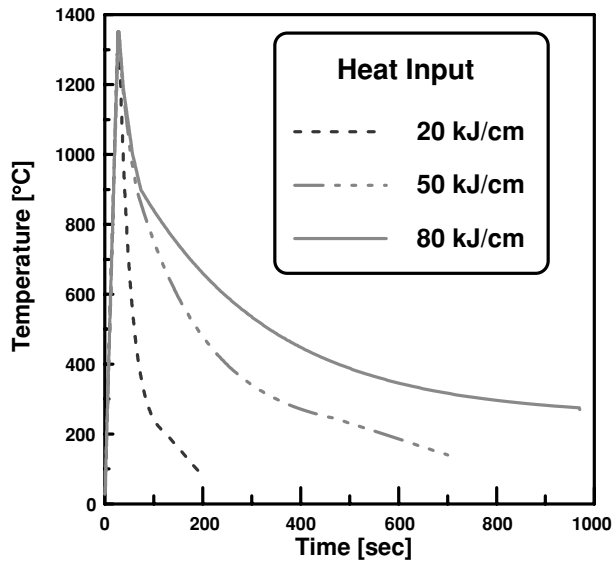

Figure 1 Thermal cycles of HAZ simulations corresponding to real thermal cycles for heat inputs with 20, 50 and 80 kJ/cm.

*Author to whom all correspondence should be addressed.
†*Present address*: Department of Mechanical Engineering, Yuan-Ze University, Chung-Li, Taoyuan, Taiwan, ROC.

TABLE I Chemical compositions of modified 2.25Cr-1Mo steels in this study (wt%)

Fe	C	Cr	Mo	Mn	V	Ti	B	Al	Si	P	S	Ni
Bal.	0.098	2.0	0.97	0.50	0.245	0.036	0.002	0.008	0.04	0.017	0.013	0.17

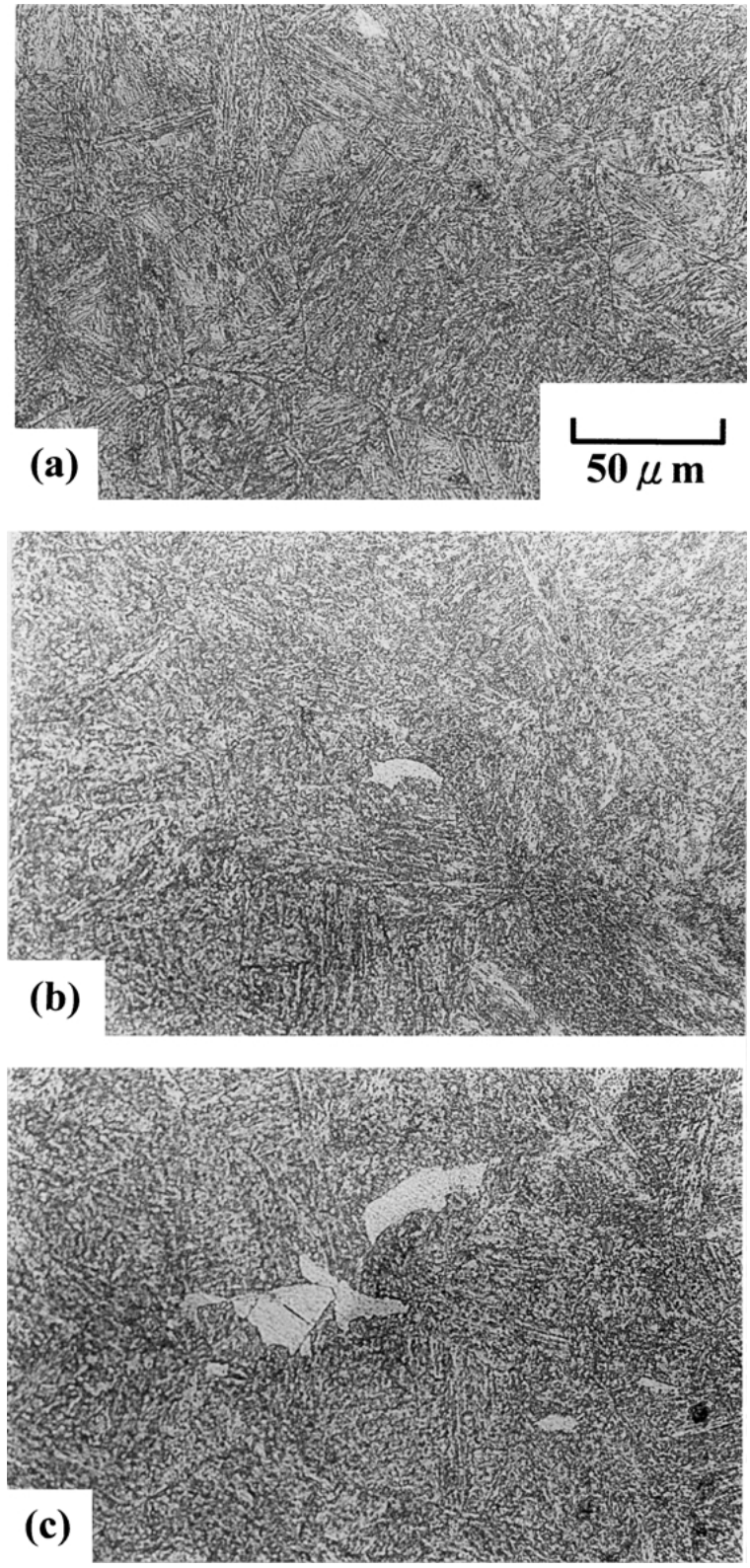

Figure 2 Optical metallographs showing microstructure obtained from the specimens after HAZ simulations corresponding to real thermal cycles for heat input with (a) 20 kJ/cm, (b) 50 kJ/cm, and (c) 80 kJ/cm.

boron nitride. Titanium carbides are also more stable than the chromium and molybdenum carbides [4].

Because modified 2.25Cr-1Mo steel possesses a high creep strength with good toughness, it has been increasingly used in the power generation for containment vessels, superheater tubes and steam pipes [5]. The welding is the necessary process during fabrication of these components. After welding, the microstructures formed in both weld metal and heat affected zone (HAZ) play an important role in controlling the mechanical properties of the weldment [6]. The heat input is definitely effective on the microstructures formed in weld metal and HAZ [7]. However, there is no detailed work on microstructural changes in modified 2.25Cr-1Mo steel during the high temperature exposure, especially in the heat-affected zone (HAZ). The purpose of this work is aimed at this aspect.

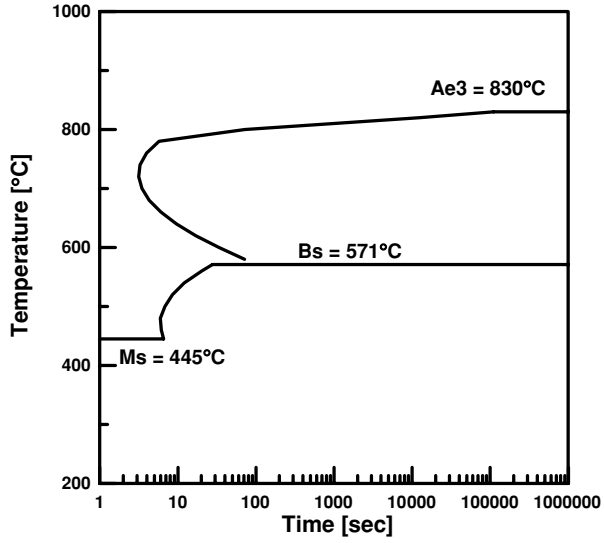

Figure 3 Calculated TTT diagram for steel studied: after Bhadeshia [8].

2. Experimental procedure

Specimens of the modified 2.25Cr-1Mo steel were received as hot-rolled bars. The composition of the steel is listed in Table I. In this work, the simulated HAZ experiments were performed on a Dilatronic III RDP deformation dilatometer of Theta Industries, Inc. Before thermal simulation, the representative weld thermal cycles of actual welding had been obtained as described below. Test beads were deposited on steel plates 20 mm thick using the bead on plate technique by submerged-arc welding with three different heat inputs, 20, 50 and 80 kJ/cm The thermal cycles were measured at the location of coarse-grained region in the HAZ close to the fusion boundary. The thermal cycles are shown in Fig. 1; the peak temperatures were approaching 1350°C for the three cycles and cooling times between 800 and 500°C $\Delta t_{8/5}$ for the heat inputs of 20, 50 and 80 kJ/cm were 16, 102 and 220 s, respectively. Before preparation of dilatometric specimens, the bars of the modified 2.25Cr-1Mo steel were homogenized at 1200°C for 3 days while sealed in a quartz tube containing a partial pressure of pure argon. The specimens were machined in the form of 3 mm diameter cylindrical rods with 6 mm length. The dilatometer was connected to a computer workstation with a PDP 11/55 central processor to analyze the resulting data. A software package (also provided by theta Industries) can give a flexible environment to execute identical thermal cycles for HAZ simulation. The length, time and temperature information can be recorded at microsecond intervals and the level of vacuum can reach 10^{-5} torr to protect specimens from oxidation. The high-temperature exposures for simulated HAZ specimens were carried out at 700°C for 1, 2, 5, 10, 20, 50, 100, 200 and 500 h in a air furnace, while the specimens being sealed in quartz capsules under a partial pressure of argon.

The specimens for optical metallography were prepared from dilatometer specimens and high-temperature exposured specimens. They were mechanically polished and then etched in 2% nital solution. Transmission electron microscopy (TEM) specimens were prepared from 0.25 mm thick discs. The discs were thinned to 0.07 mm by abrasion on SiC papers

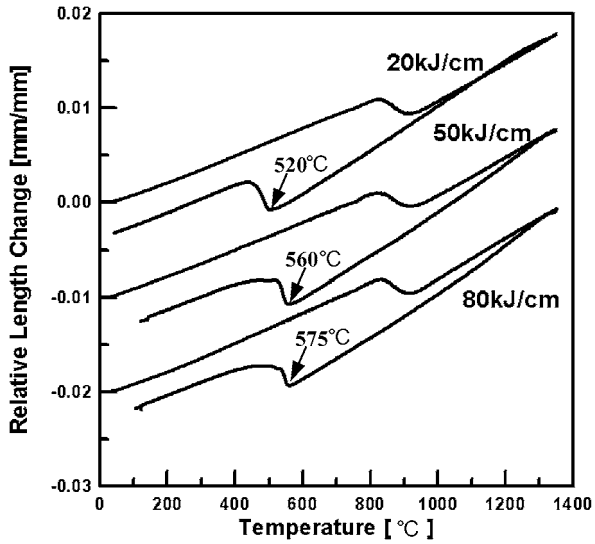

Figure 4 Dilatometric curves for the simulated course-grained HAZ with heat input 20, 50 and 80 kJ/cm.

and then twin-jet electropolished using a mixture of 5% perchloric acid, 25% glycerol, and 70% ethanol at room temperature, using a 60 V polishing potential. They were examined using a JEM-100CX II transmission electron microscope operated at 100 kV.

Carbon extraction replicas were prepared from specimens that had been polished for optical microscopy. The specimens were heavily etched in 2% nital solution, and then a carbon film (about 15–30 nm in thickness) was deposited by evaporation. The carbon film of the specimen was scored with a sharp knife into a 1.5 mm square grid pattern, etched again with 5% nital solution to dissolve the matrix, and then the replicas were "floated off" on the surface of ethanol. Finally,

TABLE II The phase transformation start temperature and finish temperature measured from Fig. 4

	Heat input		
Transformation	20 (kJ/cm)	50 (kJ/cm)	80 (kJ/cm)
Start temperature (°C)	520	560	575
Finish temperature (°C)	405	390	385

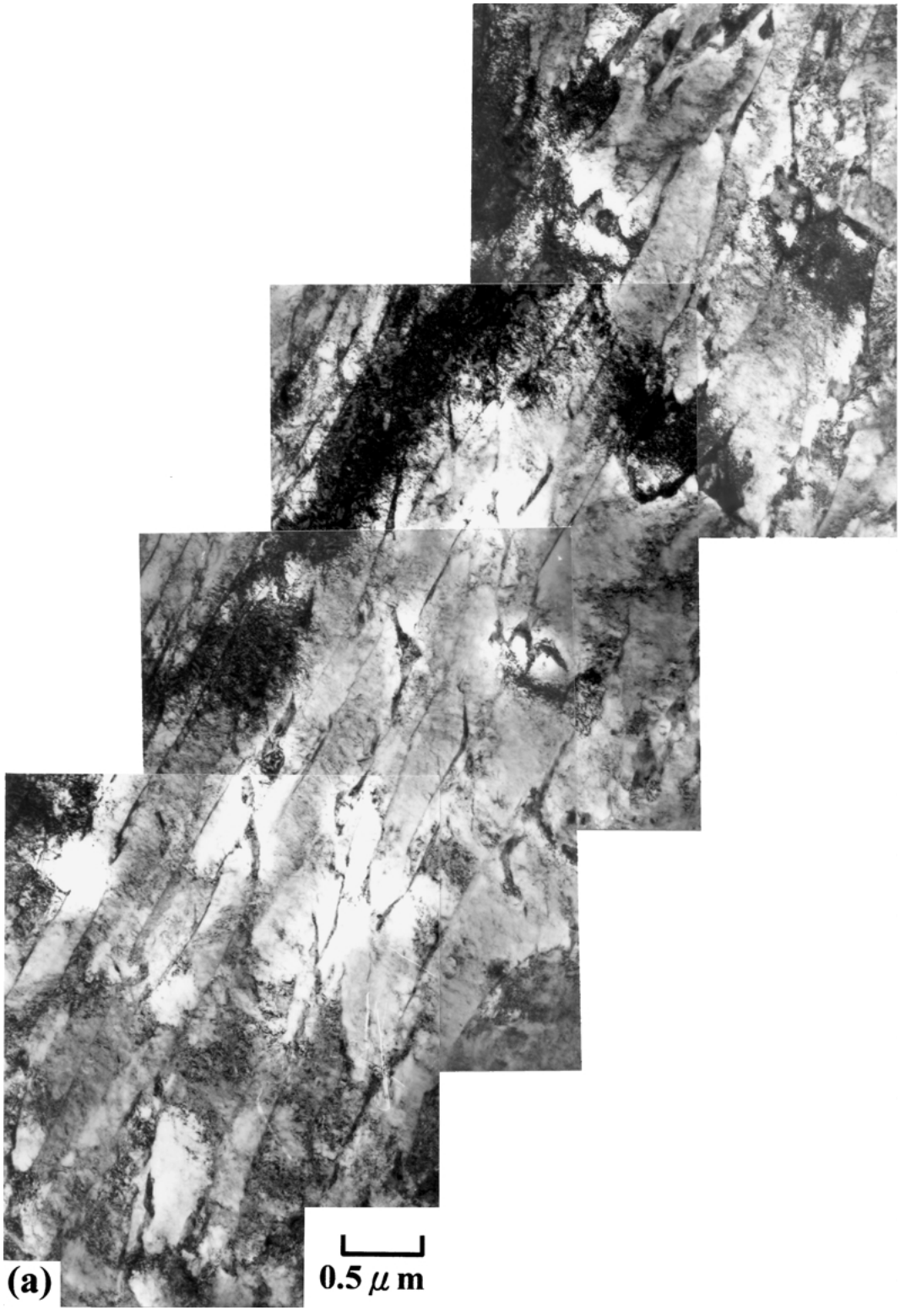

Figure 5 Transmission electron micrographs obtained from 20 kJ/cm heat input specimen. (a) Lower bainite structure and (b) martensitic structure. (*Continued*)

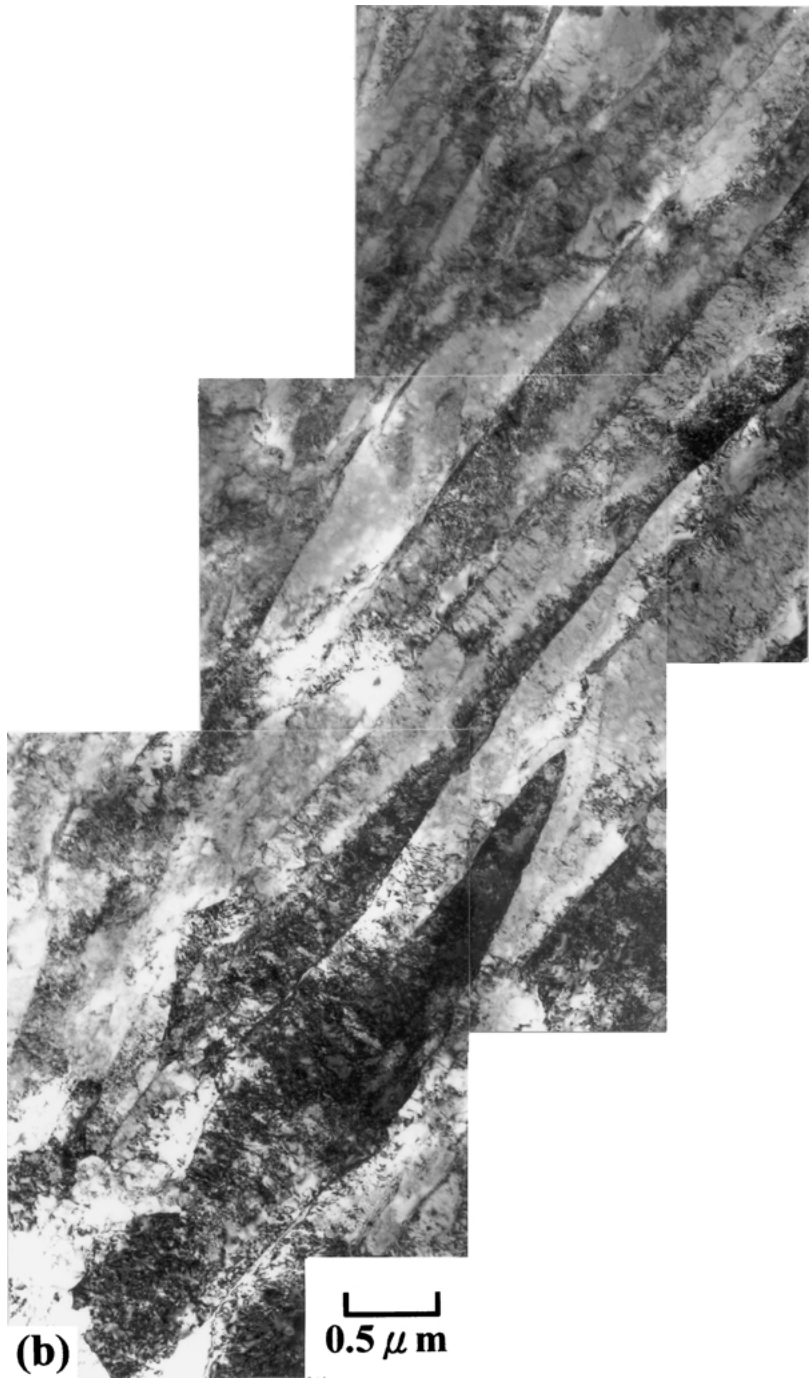

Figure 5 (*Continued*).

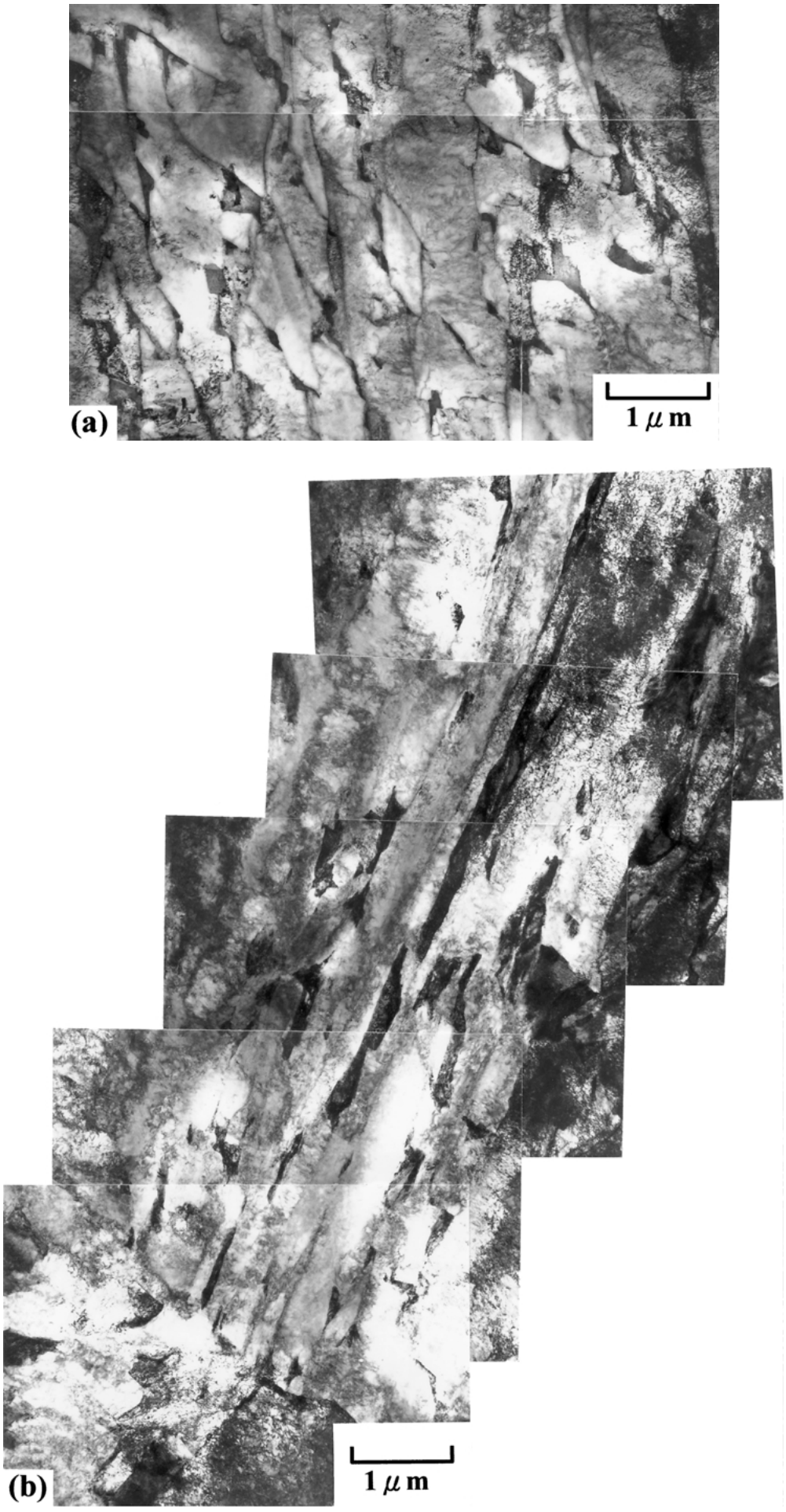

Figure 6 Transmission electron micrographs obtained from 50 kJ/cm heat input specimen. (a) Lower bainitic structure, (b) upper bainitic structure, and (c) allotriomorphic structure. (*Continued*)

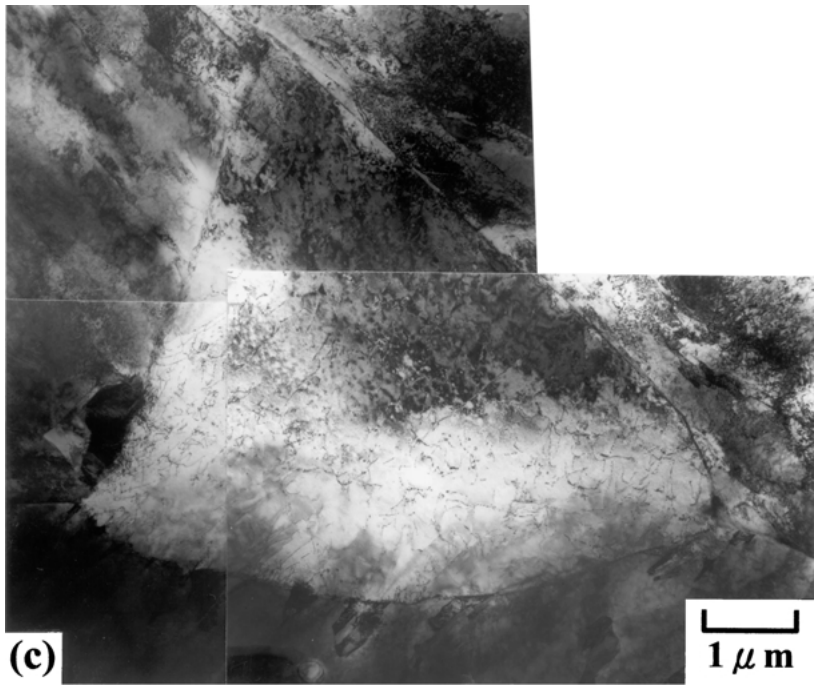

Figure 6 (*Continued*).

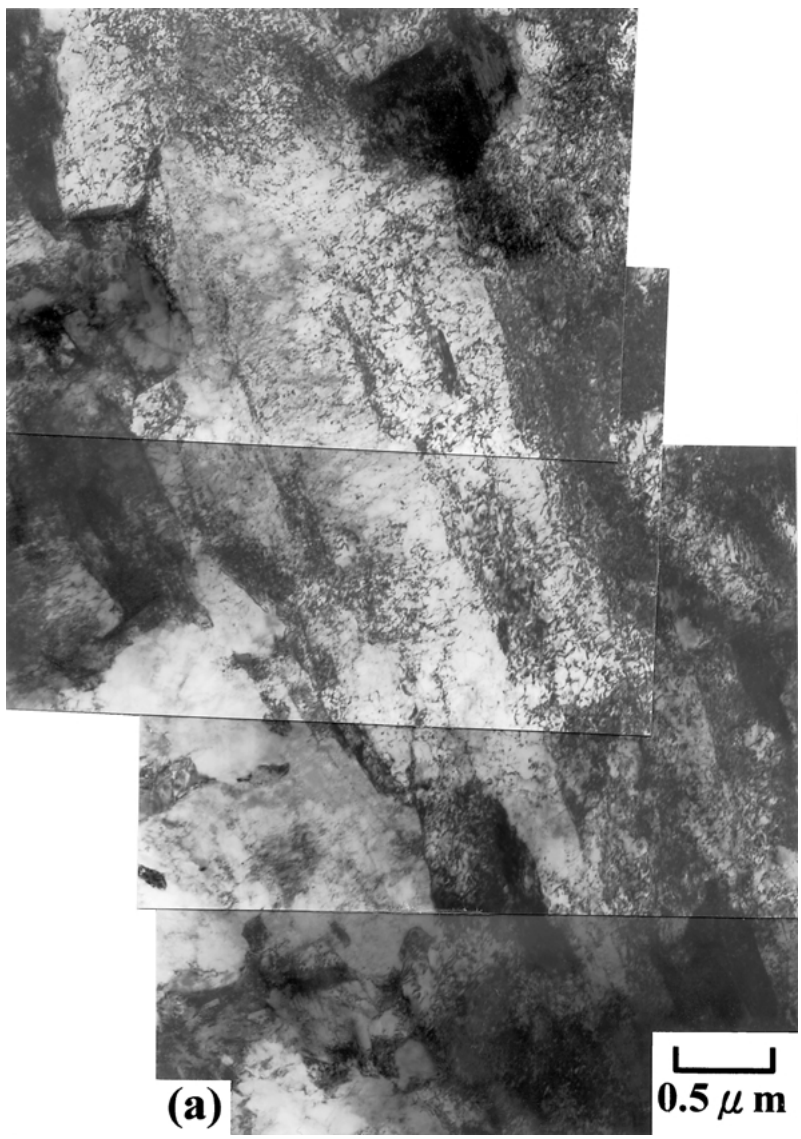

Figure 7 Transmission electron micrographs obtained from 80 kJ/cm heat input specimen. (a) Upper bainitic structure, (b) mixture of upper and lower bainitic structure, and (c) allotriomorphic structure. (*Continued*)

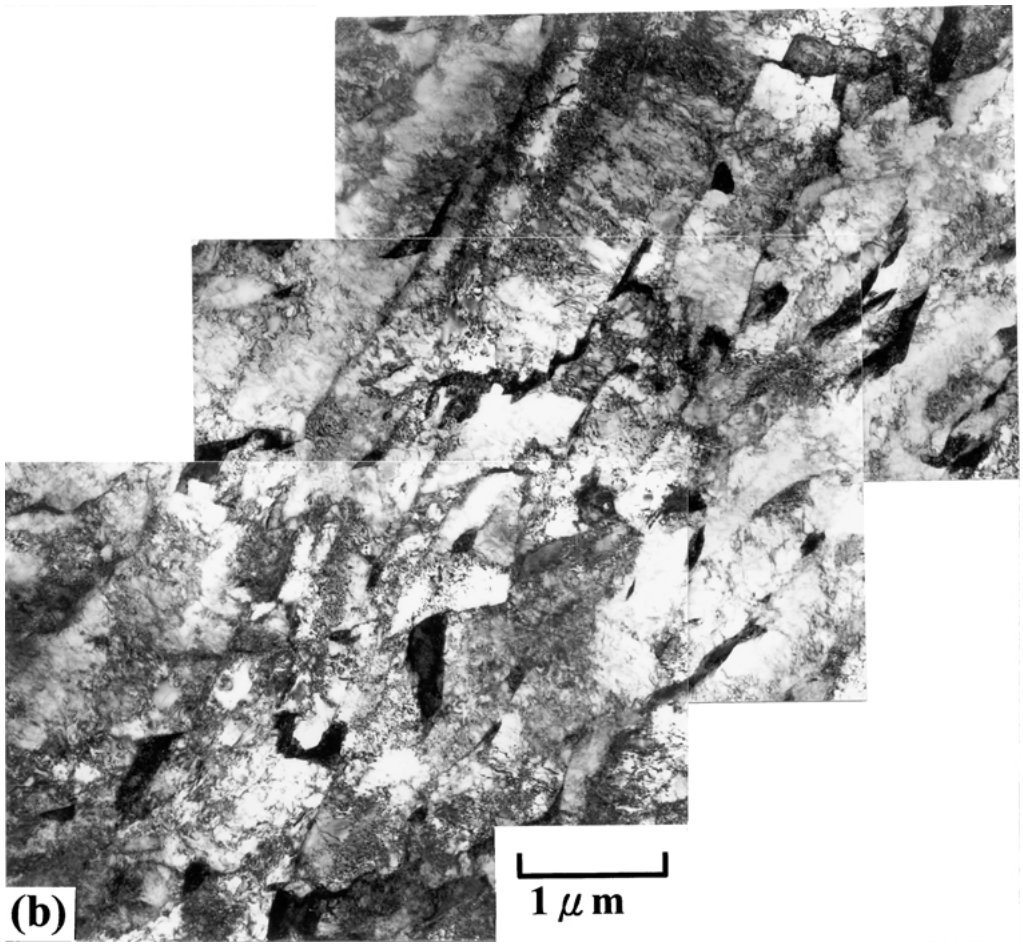

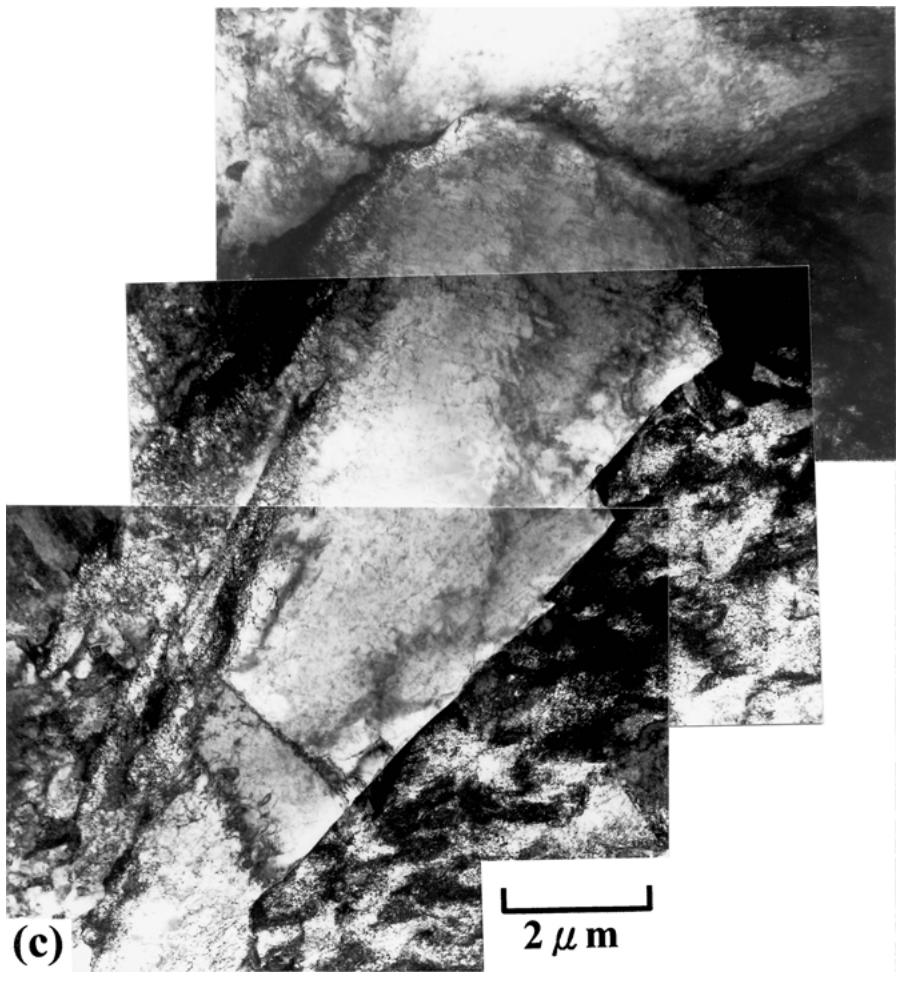

Figure 7 (*Continued*).

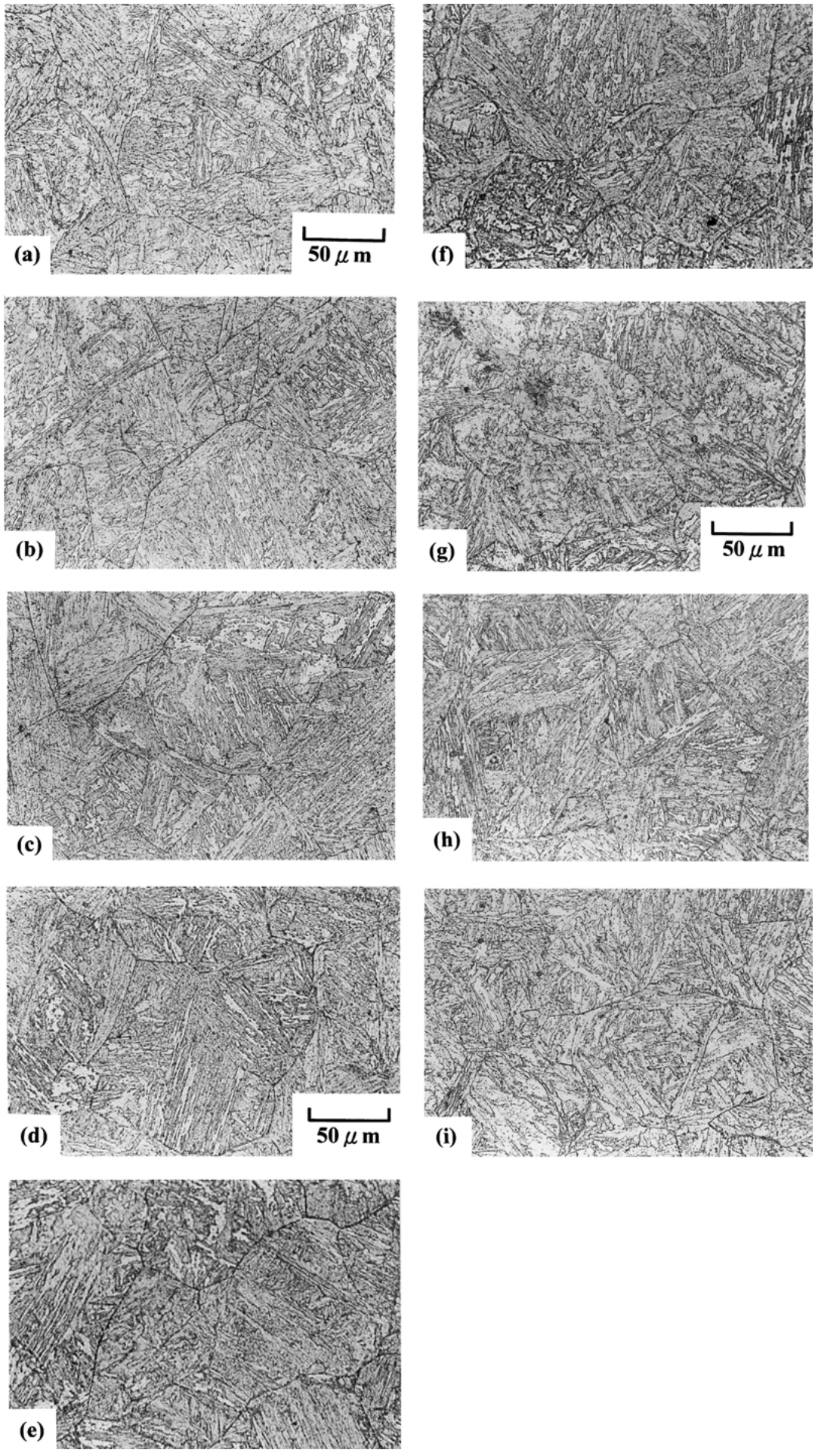

Figure 8 Optical micrographs of specimens tempered at 700°C for (a) 1 h, (b) 2 h, (c) 5 h, (d) 10 h, (e) 20 h, (f) 50 h, (g) 100 h, (h) 200 h, and (i) 500 h.

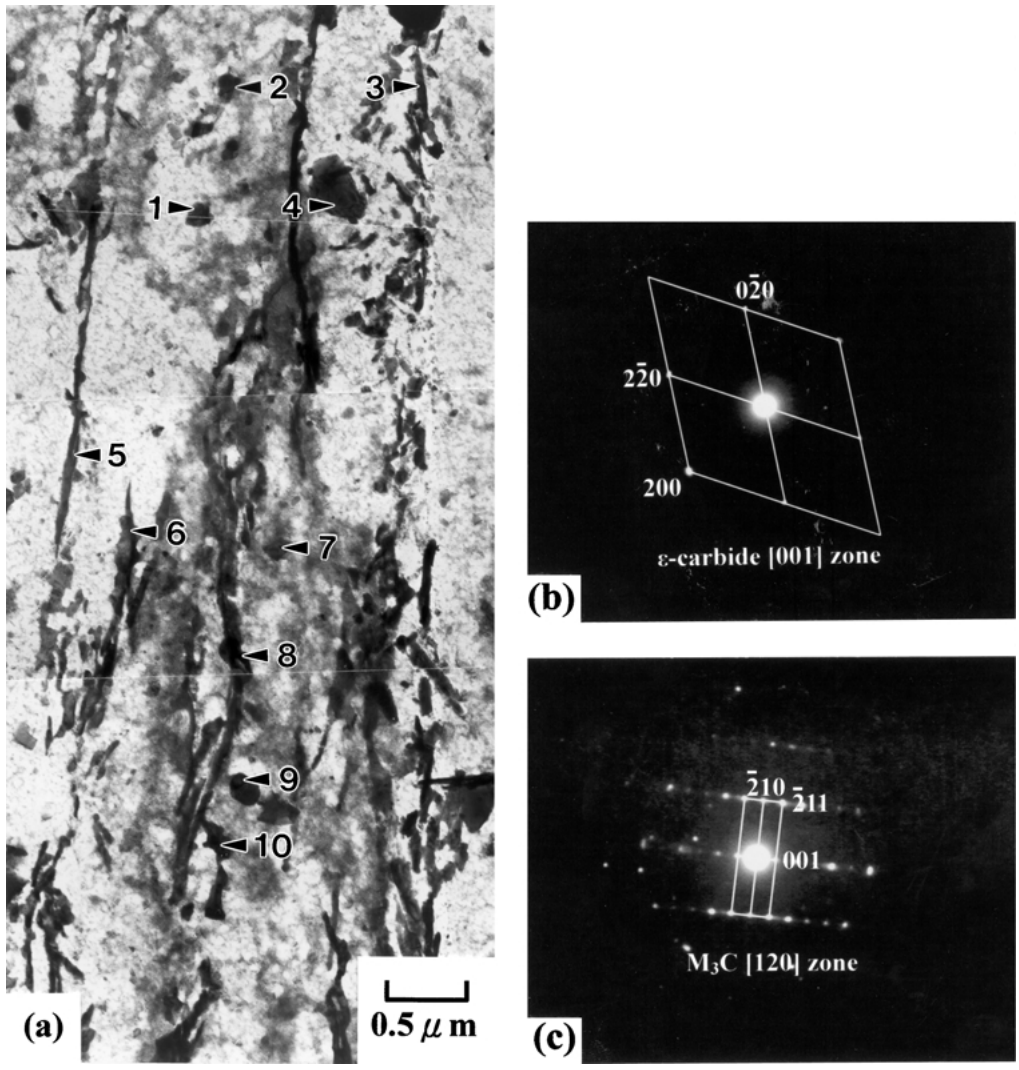

Figure 9 (a) Transmission electron micrographs of a replica showing the microstructure of bainitic region obtained from the specimen tempered at 700°C for 1 h. Corresponding diffraction patterns, (b) obtained from position 1, and (c) obtained from position 6. (The carbide at position 1 is ε-carbide and the carbides at positions 2–10 are M_3C.)

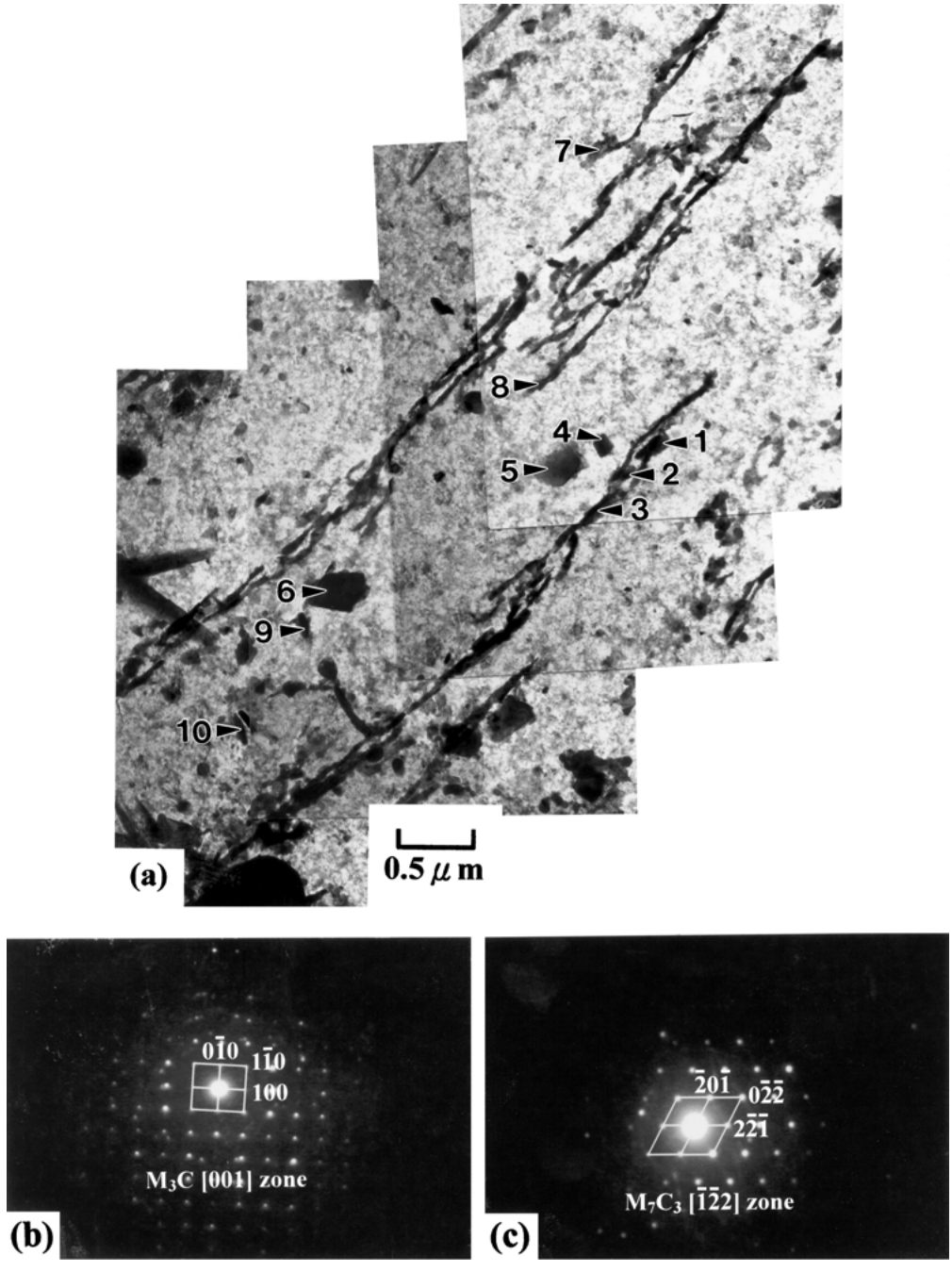

Figure 10 (a) Transmission electron micrographs of a replica showing the microstructure of bainitic region obtained from the specimen tempered at 700°C for 5 h. Corresponding diffraction patterns, (b) obtained from position 1, and (c) obtained from position 10. (The carbides at positions 1–6 are M_3C and the carbides at positions 7–10 are $M7C_3$.)

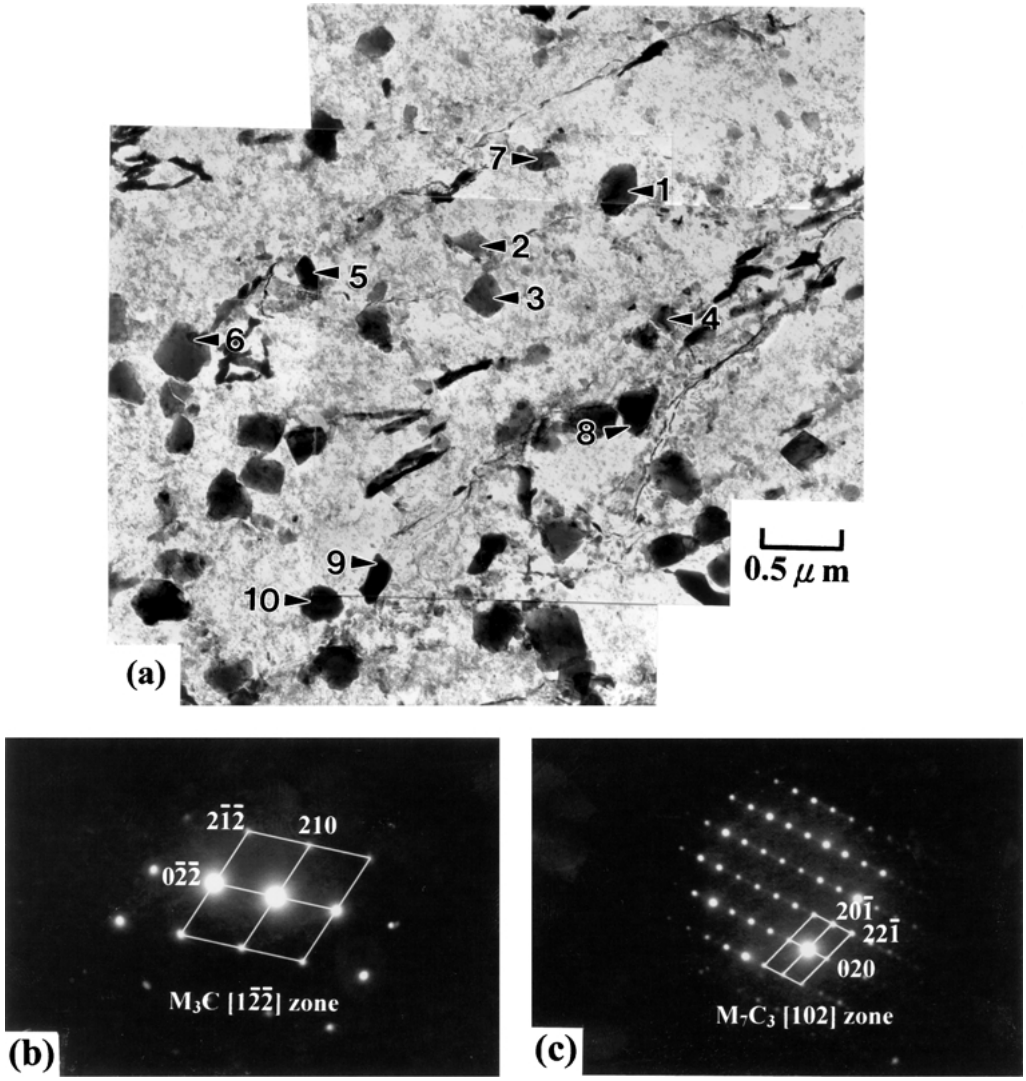

Figure 11 (a) Transmission electron micrographs of a replica showing the microstructure of bainitic region obtained from the specimen tempered at 700°C for 20 h. Corresponding diffraction patterns, (b) obtained from position 2, and (c) obtained from position 10. (The carbides at positions 1–6 are M_3C and the carbides at positions 7–10 are M_7C_3.)

the replicas were picked up on copper grids and dried on filter paper. To investigate the morphology, size distribution, and crystal structure of carbides, the replicas were examined on JEM-2000EX scanning transmission electron microscope with energy dispersive x-ray spectrometer (STEM-EDS) operated at 200 kV.

3. Results and discussion

To investigate the effect of heat input on the microstructural constituents in the modified 2.25Cr-1Mo steel, three different thermal simulations were carried out on a dilatometer for optical metallograph specimens and transmission electron micrograph specimens. Simulated HAZ thermal cycles (Fig. 1) were carried out and the corresponding optical microstructures are shown in Fig. 2.

In order to elucidate the simulated HAZ microstructures, further investigation of the time-temperature-transformation (TTT) diagram and by TEM were carried out. Fig. 3 shows the calculated TTT diagram, based on the model developed by Bhadeshia [8]. In such a diagram, the upper C curve represents the time taken for the initiation of diffusion transformations such as allotriomorphic ferrite and pearlite, whereas the lower C curve represents the time taken for the initiation of displacive transformation such as bainite [9–12]. The TTT diagram shows that the martensite start temperature (Ms) is about 445°C and the bainite start temperature (Bs) about 571°C. The dilatometric curves for simulated HAZ specimens with 20, 50 and 80 kJ/cm are presented in Fig. 4. The corresponding transformation start and finish temperatures during cooling for these three thermal cycles are listed in Table II. The simulated 20 kJ/cm heat input specimen gives martensite and lower bainite; the simulated 50 kJ/cm heat input microstructure was composed of upper bainite, lower bainite and martensite; In addition, the simulated 80 kJ/cm heat input microstructure consisted of allotriomorphic ferrite, upper bainite, lower bainite and martensite.

The optical micrograph of Fig. 2a obtained from 20 kJ/cm heat input specimen shows the sheaf-like structure, which cannot be resolved the details by optical microscope. The corresponding transmission electron micrographs are shown in Fig. 5. Fig. 5a shows the typical microstructure of the lower bainite which is characteristic with intraplate carbides precipitated in a single variant within the sub-unit bainitic ferrite. Furthermore, Fig. 5b shows that the martensitic lath, with a thickness of about 0.5 μm, possesses a high dislocation density.

Fig. 6 shows the transmission electron micrographs obtained from 50 kJ/cm heat input specimen; the microstructures consist mainly of lower bainite, upper bainite and allotriomorphic ferrite. The evidence suggests that the gray and white etching structures in Fig. 2 should be separately bainite and allotriomorphic ferrite. Although the structure of martensite is expected to exist in the 50 kJ/cm heat input specimen, it cannot be found in TEM. The possible reason is that the volume fraction of martensitic structure is too small to be found out.

Figure 12 Transmission electron micrographs of a thin foil specimen tempered at 700°C for 20 h.

For 80 kJ/cm heat input specimen, the dilatometric data shows a wider transformation temperature range during cooling (the transformation start and finish temperatures are 575 and 385°C, respectively). The wider the transformation temperature range, the more complicated the product structures. It gives allotriomorphic ferrite, upper bainite, lower bainite and martensite as shown in Fig. 7. Fig. 7b shows the TEM micrograph containing the mixture of upper and lower bainite, but this structure does not appear to be with a typical morphology for bainite. Because the transformation temperature range was wider, the different products would interfere with each other. This makes the interpretation of microstructures difficult. Fig. 7c shows the block-shaped allotriomorphic ferrite on the prior-austenite boundary; the ledges on the allotriomorphic

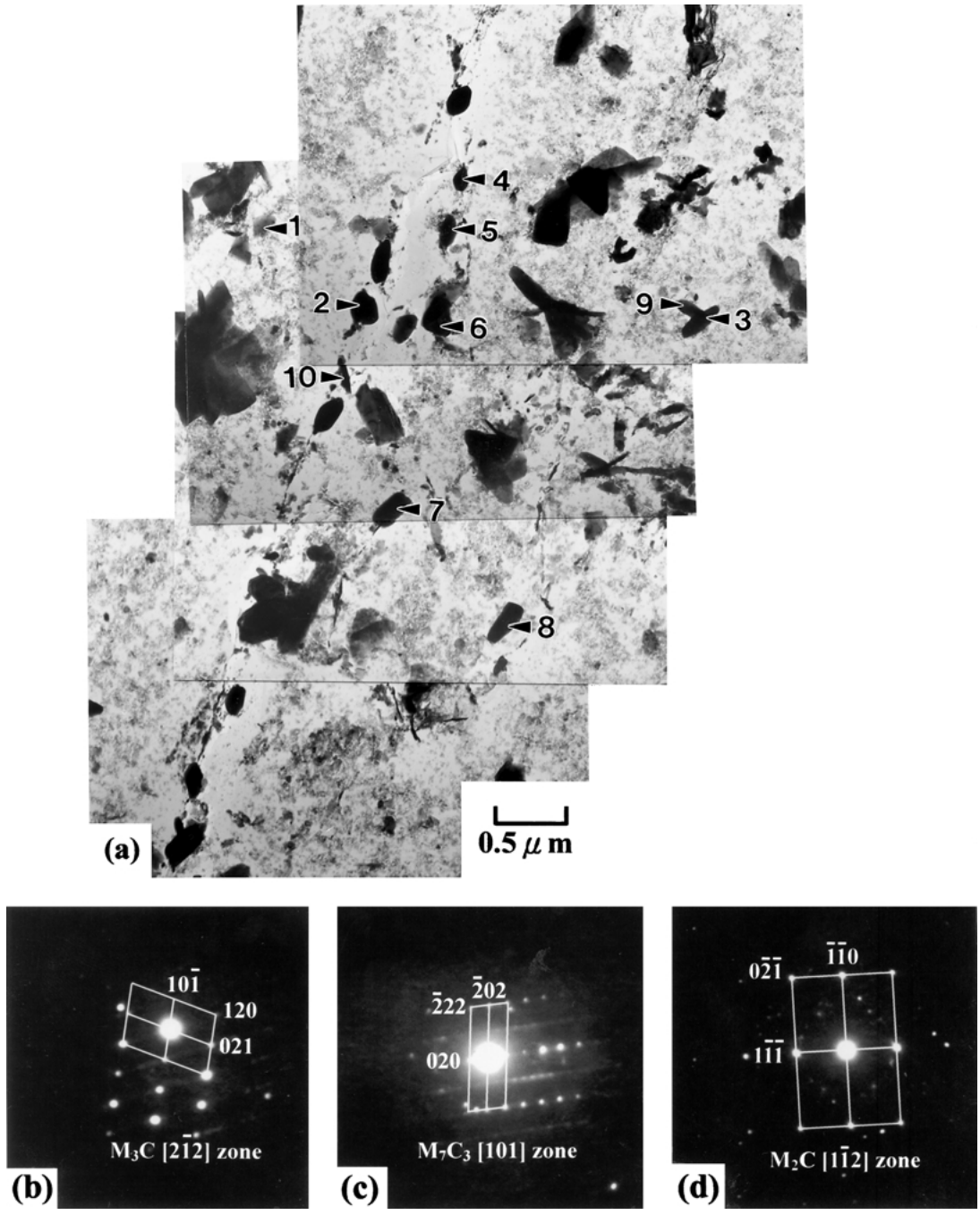

Figure 13 (a) Transmission electron micrographs of a replica showing the microstructure of bainitic region obtained from the specimen tempered at 700°C for 50 h. Corresponding diffraction patterns, (b) obtained from position 3, (c) obtained from position 5, and (d) obtained from position 9. (The carbides at positions 1–3 are M_3C, the carbides at positions 4–8 are M_7C_3 and the carbides at positions 9–10 are M_2C.)

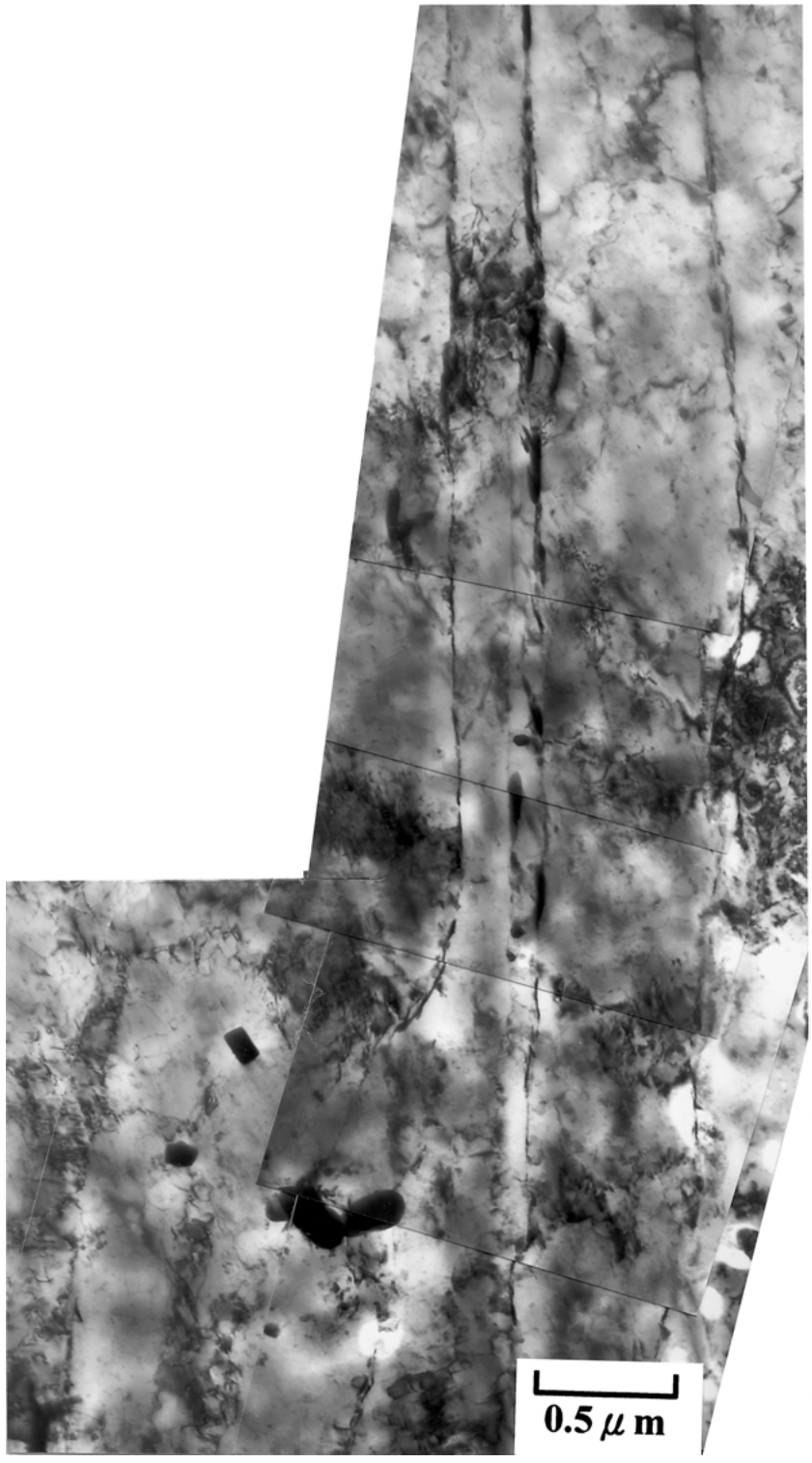

Figure 14 Transmission electron micrographs of a thin foil specimen tempered at 700°C for 50 h.

ferrite boundary can be seen clearly. The formation of allotriomorphic ferrite crossing the grains of the parent phase is with the diffusive mechanism instead of the displacive mechanism.

In order to study the microstructure degeneration of bainitic structure, the tempering experiments had been carried out at 700°C for different time intervals (1, 2, 5, 10, 20, 50, 100, 200 and 500 h) in the 20 kJ/cm heat input specimens. The corresponding metallographs are shown in Fig. 8; they do not reveal any clear change in the microstructures during the stages of tempering. For the purpose of investigating carbide transformations, the carbon extract replicas had been investigated. Fig. 9 shows the TEM micrograph of replica of lower bainitic structure tempered at 700°C for 1 h; the original morphology of sheet-like carbides (within the bainitic sub-units) became rounded. The diffraction patterns have been analyzed to identify the type of carbides; they reveal the epsilon carbide (ε-carbide) and M_3C particles situated within sub-units, and the film shaped M_3C located at the boundaries of sub-units. In the specimen tempered at 700°C for 5 h (Fig. 10), the coarse M_3C carbides within bainitic sub-unit and some of finer precipitates M_7C_3 carbides along the boundary and within bainitic subunit can be found. Fig. 11 shows TEM micrograph obtained from the specimen tempered at 700°C for 20 h; most of the coarse carbides (the majority of carbides are M_7C_3 and others are M_3C carbides) were distributed within bainitic subunit. Fig. 12 shows the TEM structure for the specimen tempered at 700°C

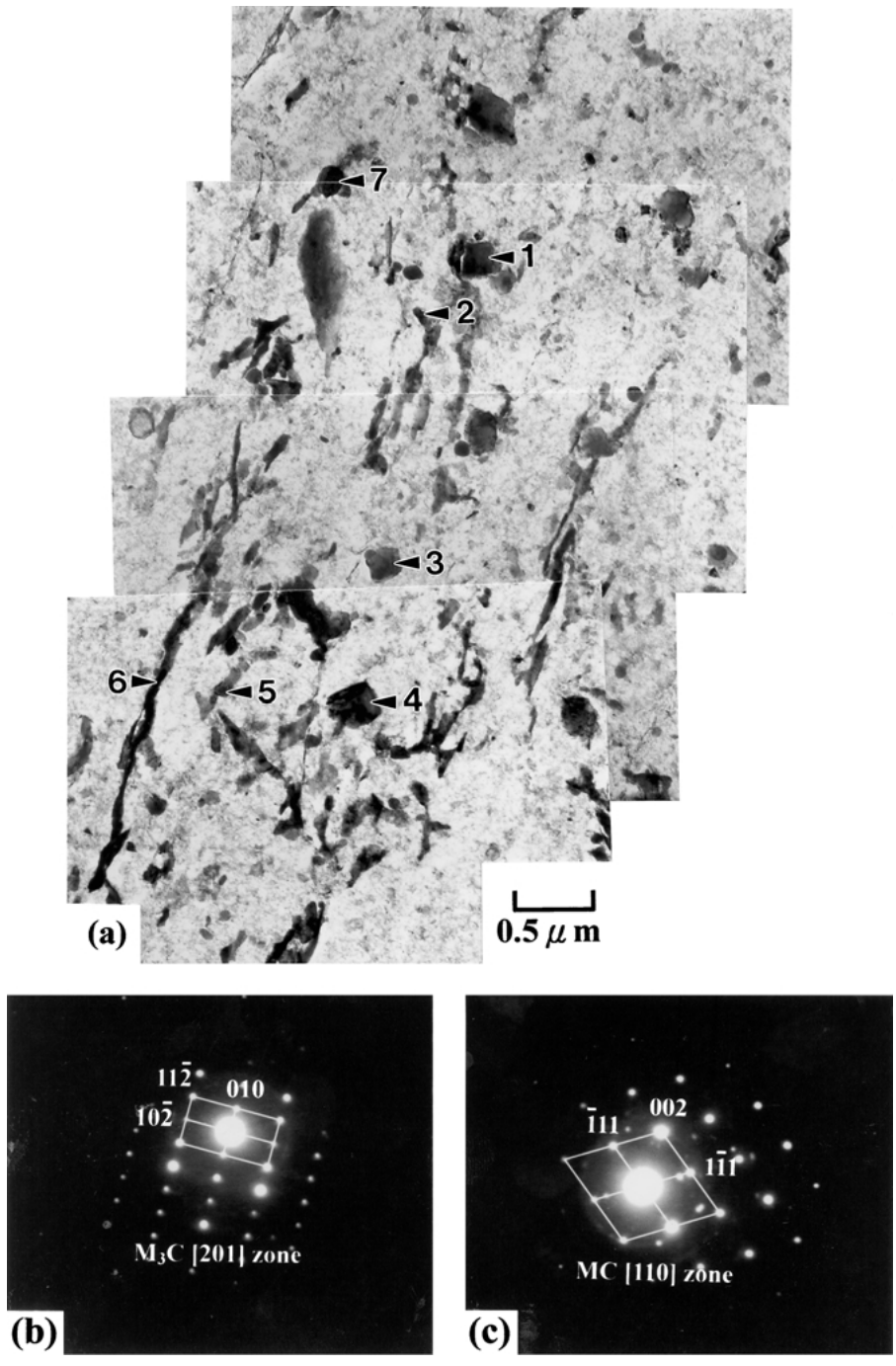

Figure 15 (a) Transmission electron micrographs of a replica showing the microstructure of bainitic region obtained from the specimen tempered at 700°C for 200 h. Corresponding diffraction patterns, (b) obtained from position 6, and (c) obtained from position 7. (The carbides at positions 1–6 are M_3C and the carbide at positions 7 is MC.)

for 20 h; it indicates some areas of upper bainite have been recoveried. In the specimen tempered at 700°C for 50 h (Fig. 13), the fine M_2C particles can be detected but their amount is very few. Transmission electron microscopy (Fig. 14) clearly shows that the cell structures from within the bainitic sub-unit lath at this tempering condition.

Finally, the micrograph of specimens tempered at 700°C for 200 h and 500 h are shown in Figs 15 and 16 respectively. Because of the microalloying (V, Ti and B) addition in this steel, the precipitation of MC (i.e. (V,Ti)C or V_4C_3 in this steel) could occur during tempering and it could prevent the formation of $M_{23}C_6$ carbides. It has been claimed that Mo, Ti, V and Nb elements cause the $M_{23}C_6$ carbides to be unstable and decrease their energies [13]. This proposal is in agreement with the result in the present work, i.e., no the $M_{23}C_6$ carbides had been detected. The MC carbide is an important strengthening phase in many tool steels because it would increase the toughness and strength in high temperatures [14]. Virostkova *et al*. investigated the carbide transformation in Cr-Mo-V steel that the compositions of vanadium are in the range 0.02–0.34 wt% [15, 16]. They suggested that the MC carbide could formed in the Cr-Mo steel, with more than 0.12 wt% Vanadium, tempered at 660°C for 15 h. In this study, the

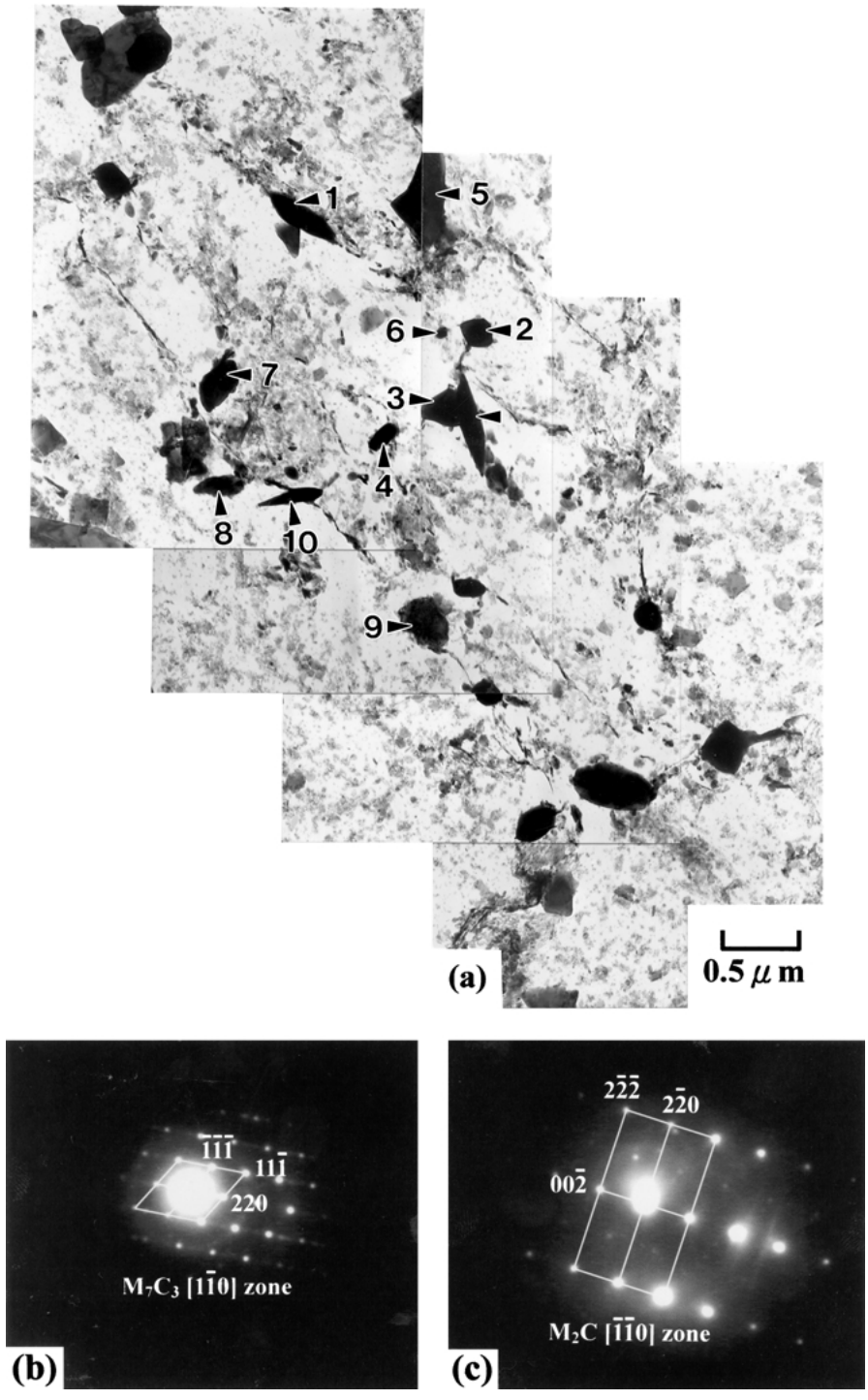

Figure 16 (a) Transmission electron micrographs of a replica showing the microstructure of bainitic region obtained from the specimen tempered at 700°C for 500 h. Corresponding diffraction patterns, (b) obtained from position 3, and (c) obtained from position 5. (The carbides at positions 1–4 are M_7C_3 and the carbides at positions 5–10 are M_2C.

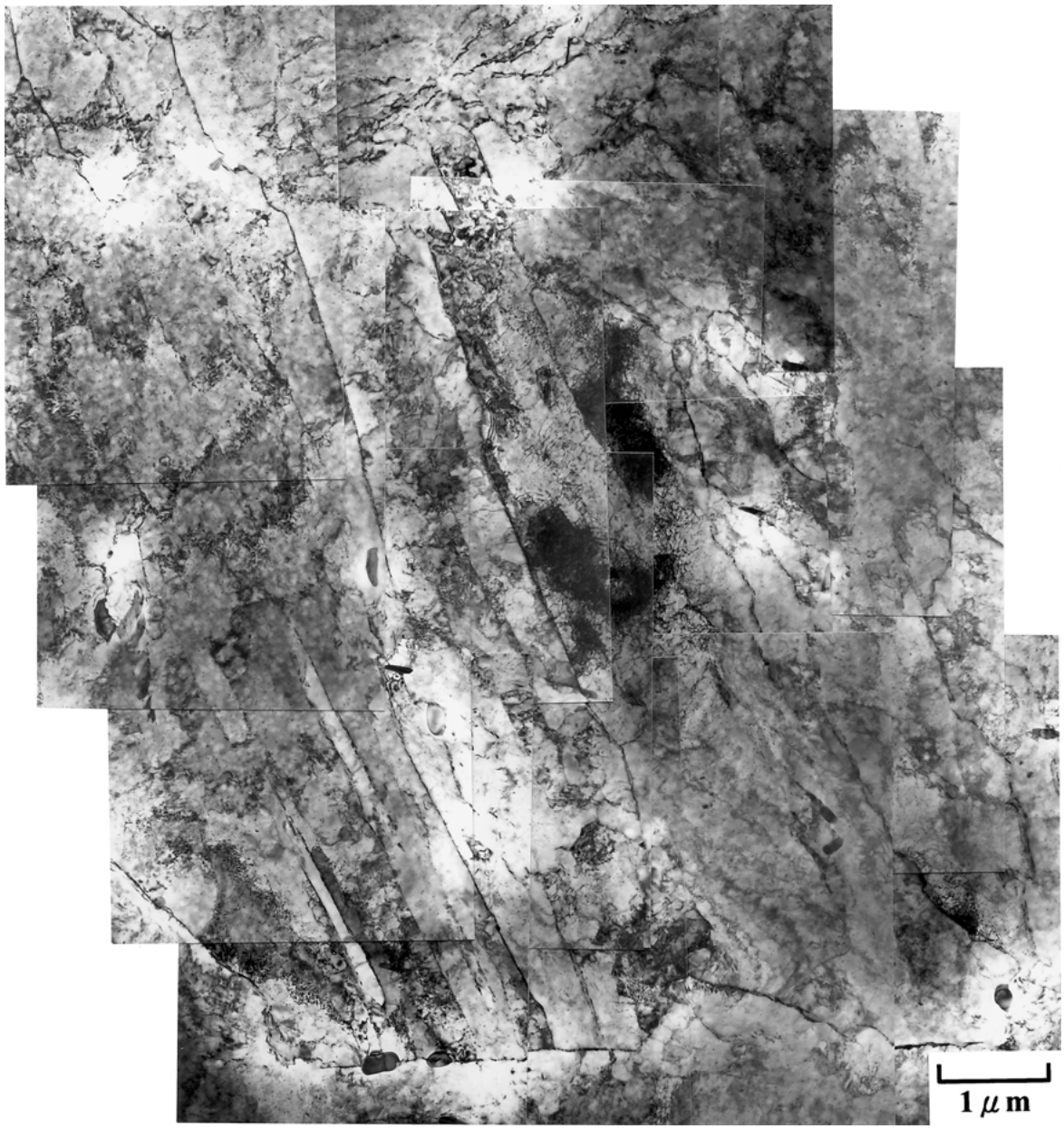

Figure 17 Transmission electron micrographs of a thin foil specimen tempered at 700°C for 500 h.

level of vanadium was 0.245 wt%, the MC was found after the specimen was tempered at 700°C for 200 h; however, the amount of MC was very few. It could be suggested that the MC carbide formed in earlier tempering stage with a extremely small size that could not be detected by the conventional TEM diffraction analysis. After specimen was tempered for 500 h, the carbides exist as the type of M_2C (about 70% volume fraction of the total carbides) and that of M_7C_3 (30% volume fraction). It should be noted that the bainitic ferrite plates were less affected even after tempering at 700°C for 500 h (Fig. 17); the bainite still could keep its characteristic plate morphology. The result reflect that the tempering response is less sensitive in bainite than in martensite.

4. Conclusions

1. After the simulated welding with heat input of 20 kJ/cm, the microstructures consist mainly of lower bainite with a few amounts of martensite and upper bainite. In the case of specimen with heat input of 50 kJ/cm, the microstructures are composed of lower bainite, upper bainite and a few amount of allotriomorphic ferrite. In the simulated heat input of 80 kJ/cm specimen, lower bainite, upper bainite with a few amount of martensite and allotriomorphic ferrite can be obtained.

2. The phenomena of recovery was observed in the 20 kJ/cm simulated HAZ specimen after tempering at 700°C for 50 h, but the recrystallization still did not occur in the 20 kJ/cm simulated HAZ specimen after tempering at 700°C for 500 h.

3. The precipitation sequence of carbides in the 20 kJ/cm simulated HAZ specimen during tempering at 700°C can be proposed as follows:

$$\begin{Bmatrix}\varepsilon-\text{carbide}\\ M_3C\end{Bmatrix} \xrightarrow{2\,h} M_3C \xrightarrow{5\,h} \begin{Bmatrix}M_3C\\ M_7C_3\end{Bmatrix} \xrightarrow{50\,h} \begin{Bmatrix}M_3C\\ M_7C_3\\ M_2C\end{Bmatrix}$$

$$\xrightarrow{200\,h} \begin{Bmatrix}M_3C\\ MC\end{Bmatrix} \xrightarrow{500\,h} \begin{Bmatrix}M_7C_3\\ M_2C\end{Bmatrix}$$

References

1. J. R. DAVIS *et al.* (eds.), "Metals Handbook," Vol. 1, 10th ed. (ASM International, USA, 1990) p. 617.
2. R. L. KLUEH and R. W. SWINDEMAN, *Metallurgical Transaction* A **17A** (1986) 1027.
3. J. YU and C. J. MCMAHON, Jr., *ibid.* **11A** (1980) 277.
4. W. B. JONES, C. R. HILLS and D. H. POLONIS, *ibid.* **22A** (1991) 1049.
5. H. K. D. H. BHADESHIA, "Bainite in Steels" (The Institute of Materials, London, 1992) p. 329.
6. W. H. REARNS (ed.), "Welding Handbook, Metals and Their Weldability" Vol 4. (American Welding Society, Miami, FL, 1980).
7. M. EROGLU, M. AKSOY and N. ORHAN, *Materials Science and Engineering* A **269** (1999) 59.
8. H. K. D. H. BHADESHIA, *Metal Science* **16** (1982) 159.
9. *Idem.*, *Acta. Metallurgica* **29** (1981) 1117.
10. A. ALI and H. K. D. H. BHADESHIA, *Materials Science and Technology* **6** (1990) 781.
11. H. K. D. H. BHADESHIA, "Bainite in Steels" (The Institute of Materials, London, 1992) p. 126.
12. A. ALI and H. K. D. H. BHADESHIA, *Materials Science and Technology* **7** (1991) 895.
13. V. KUZUCU, M. AKSOY and M. H. KORKUT, *Journal of Materials Processing Technology* **82** (1998) 165.
14. H. M. WANG, L. G. YU, X. X. LI and P. JIANG, *Science and Technology of Advanced Materials* **2** (2001) 173.
15. A. VYROSTKOVA, A. KROUPA, J. JANOVEC and M. SVOBODA, *Acta Mater* **46**(1) (1998) 31.
16. A. KROUPA, A. VYROSTKOVA, M. SVOBODA and J. JANOVEC, *ibid.* **46**(1), (1998) 39.

Received 11 July
and accepted 12 November 2002